Letter

Majorana parameters of the interacting boson model of nuclear structure and their implication for $0\nu\beta\beta$ decay

J. Kleemann,[1,*] T. Beck,[1,†] U. Friman-Gayer,[1,‡] N. Pietralla,[1] V. Werner,[1] S. W. Finch,[2] J. Kotila,[3,4] Krishichayan,[2] B. Löher,[1] H. Pai,[1,§] O. Papst,[1] W. Tornow,[2] M. Weinert,[5] and A. Zilges[5]

[1]*Institut für Kernphysik, Technische Universität Darmstadt, Schlossgartenstrasse 9, 64289 Darmstadt, Germany*

[2]*Department of Physics, Duke University and Triangle Universities Nuclear Laboratory, Durham, North Carolina 27708-0308, USA*

[3]*Finnish Institute for Educational Research, University of Jyväskylä, P.O. Box 35, 40014 Jyväskylä, Finland*

[4]*Center for Theoretical Physics, Sloane Physics Laboratory, Yale University, New Haven, Connecticut 06520-8120, USA*

[5]*Institut für Kernphysik, University of Cologne, Zülpicher Strasse 77, 50937 Cologne, Germany*

(Received 23 June 2021; accepted 10 November 2021; published 10 December 2021)

The well-known spherical-deformed-transitional nucleus and potential $0\nu\beta\beta$ emitter ^{150}Nd and its daughter ^{150}Sm were investigated in nuclear resonance fluorescence experiments using quasimonoenergetic, linearly polarized γ-ray beams. For both nuclei transitions from the 1^+ scissors mode to the 0_2^+ and 2_2^+ states were observed for the first time and their respective $M1$ transition strengths were determined. Through a systematic investigation, a sensitivity of these transition strengths to the three Majorana parameters of the interacting boson model-2 (IBM-2) was established. In combination with the novel experimental data, this poses strong constraints to the Majorana parameters in improved IBM-2 representations of both nuclei. A subsequent recalculation of the nuclear matrix elements (NMEs) for the $^{150}\mathrm{Nd} \rightarrow {}^{150}\mathrm{Sm}$ $0\nu\beta\beta$ decay in the IBM-2 with these improved representations results in $M^{(0\nu\beta\beta)}_{\mathrm{IBM\text{-}2}}[0_1^+] = 3.35$ for the NME for $0\nu\beta\beta$ decay into the ground state of ^{150}Sm and $M^{(0\nu\beta\beta)}_{\mathrm{IBM\text{-}2}}[0_2^+] = 1.30$ for $0\nu\beta\beta$ decay to its 0_2^+ state.

DOI: 10.1103/PhysRevC.104.L061302

Neutrinoless double beta ($0\nu\beta\beta$) decay is a hypothesized, extremely rare, and still unobserved process [1,2] which gained much attention in the recent years with numerous large-scale experiments being dedicated to its discovery [3]. As $0\nu\beta\beta$ decay is only viable if neutrinos are Majorana fermions, its observation would immediately prove this character. Furthermore, the so-far elusive neutrino mass can be extracted from $0\nu\beta\beta$-decay rates $\lambda^{(0\nu\beta\beta)}$ by the relation

$$\lambda^{(0\nu\beta\beta)} = G^{(0\nu\beta\beta)}|M^{(0\nu\beta\beta)}|^2\langle m_\nu\rangle^2, \tag{1}$$

in which $\langle m_\nu\rangle$ is the effective neutrino mass, $G^{(0\nu\beta\beta)}$ is an exactly calculable phase-space integral [4], and $M^{(0\nu\beta\beta)}$ is a nuclear matrix element (NME). Hence, in particular, the NME has to be calculated with sufficient accuracy from nuclear structure theory to facilitate a meaningful determination of the neutrino mass from a measured decay rate. Frameworks used so far for $0\nu\beta\beta$-NME calculations include the nuclear shell model, quasiparticle random-phase approximation, energy density-functional (EDF) methods, and the interacting boson model-2 (IBM-2) [5]. However, their individual results tend to differ significantly [5]. It is, hence, of interest to further constrain theory through suitable nuclear structure observables in order to obtain more reliable calculations [6] because an accurate calculation of the NME naturally requires any theoretical framework to reproduce the nuclear structure of mother and daughter in question. In this regard the shape-phase transitional $N \approx 90$ nuclei are especially challenging, due to their location in between the spherical and well-deformed configurations on the nuclear chart, where the nuclear structure undergoes rapid changes [7]. A prime example of transitional nuclei and furthermore a potential $0\nu\beta\beta$ emitter is ^{150}Nd, which has already been established as being located very close to the critical point of this quantum phase-shape transition [8]. In comparison, its $0\nu\beta\beta$ decay daughter ^{150}Sm is more vibrator-like, yet still transitional through its proximity to the critical point situated around ^{152}Sm for the Sm isotopes [9]. Hence, the shape-phase transition turns the $^{150}\mathrm{Nd} \rightarrow {}^{150}\mathrm{Sm}$ $0\nu\beta\beta$ decay into a challenge for theory. However, it also makes it especially interesting for an experimental search for $0\nu\beta\beta$ decay: EDF theory calculations predict an enhanced $0\nu\beta\beta$ decay of ^{150}Nd into the 0_2^+ state of ^{150}Sm with a NME of $M^{(0\nu\beta\beta)}_{\mathrm{EDF}}[0_2^+] = 2.81$ [10]. Meanwhile, the NME for the $0\nu\beta\beta$ decay to the ground state (GS) of ^{150}Sm is calculated to be comparably small with $M^{(0\nu\beta\beta)}_{\mathrm{EDF}}[0_1^+] = 1.71$ [11]. This is due to an interplay of the shape-phase transition and $0\nu\beta\beta$ decay preferring decays to states of similar deformation. The GS-to-GS decay is hindered as the shape-phase transition causes differing GS

*jkleemann@ikp.tu-darmstadt.de

†Present address: Facility for Rare Isotope Beams, Michigan State University, East Lansing, Michigan 48824, USA.

‡Present address: Department of Physics, Duke University and Triangle Universities Nuclear Laboratory, Durham, North Carolina 27708-0308, USA.

§Present address: Nuclear Physics Division, Saha Institute of Nuclear Physics, 1/AF Bidhan Nagar, Kolkata 700064, India.

configurations of ^{150}Nd and ^{150}Sm [11]. At the same time, the decay to the daughter's 0_2^+ state is enhanced due to shape coexistence in the daughter, yielding a higher wave-function overlap of the daughter's 0_2^+ state with the mother's GS [10]. The larger NME for the decay into the 0_2^+ state even outweighs its smaller phase-space factor in comparison with the GS decay, yielding a decay-rate ratio of

$$\frac{\lambda^{(0\nu\beta\beta)}[0_2^+]}{\lambda^{(0\nu\beta\beta)}[0_1^+]} = 1.2$$

for $0\nu\beta\beta$ decay of ^{150}Nd according to the EDF calculation. Given that a $0\nu\beta\beta$ decay into the 0_2^+ state of ^{150}Sm will be followed by the prompt emission of two γ rays, searching for such $0\nu\beta\beta$ decays of ^{150}Nd allows the use of γ- or even $\gamma\gamma$-coincidence techniques, offering a unique experimental opportunity for significant background reduction in this case. Besides the just-discussed EDF approach, another framework well suited for nuclear structure calculations of the $N \approx 90$ nuclei [12], and hence of the NMEs of the $^{150}\text{Nd} \rightarrow {}^{150}\text{Sm}$ $0\nu\beta\beta$ decay [13], is the IBM-2 [14]. This algebraic model treats nuclei as a system of interacting proton and neutron bosons, which carry spin 0 (s boson) or 2 (d boson) and represent the pairwise coupled valence nucleons. The most recent IBM-2 calculations for the NMEs of the ^{150}Nd $0\nu\beta\beta$ decay [15] with $M_{\text{IBM-2}}^{(0\nu\beta\beta)}[0_1^+] = 3.76$ and $M_{\text{IBM-2}}^{(0\nu\beta\beta)}[0_2^+] = 0.62$ are, however, in conflict with the EDF predictions. In particular, the NME for a decay into the 0_2^+ state is much lower in the IBM-2 calculation. In a previous work on the NMEs of the $^{154}\text{Sm} \rightarrow {}^{154}\text{Gd}$ $0\nu\beta\beta$ decay, however, it was shown [10] that the IBM-2 NME calculations can strongly depend on a proper determination of the model's three so-called Majorana parameters. Unlike the other Hamiltonian parameters, an extraction of the three Majorana parameters from the experimentally observed low-lying, proton-neutron-symmetric nuclear structure alone is not feasible. Instead, information on mixed-symmetry states (MSSs) [16–18] such as the nuclear 1^+ scissors mode (ScM) [19] is required because their characteristics are dominated by the Majorana parameters in the model [20,21]. As often little or no concrete experimental information on MSSs of a specific nucleus besides their energy and GS transition strength is available, the choice of Majorana parameters is barely constrained, limiting the predictive power of IBM-2 NME calculations in these cases. In the previous work on ^{154}Gd the branching ratio of a newly observed transition of the ScM into the 0_2^+ state of ^{154}Gd was used to constrain the Majorana parameters of ^{154}Gd in the IBM-2, leading to an updated IBM-2 calculation of the respective $0\nu\beta\beta$ NME in which the $M^{(0\nu\beta\beta)}[0_2^+]$ value increased by more than an order of magnitude. Nevertheless, due to the comparably low phase-space factor for a $0\nu\beta\beta$ decay of ^{154}Sm to the 0_2^+ state of ^{154}Gd , the corresponding decay rate remains small, and ^{150}Nd was identified as a more promising candidate for a significantly large $0\nu\beta\beta$ decay rate into an excited 0^+ state. It is the purpose of this Letter to report on recent nuclear resonance fluorescence experiments on ^{150}Nd and its potential $0\nu\beta\beta$ decay daughter ^{150}Sm, which yielded novel experimental data on the $M1$ branchings of the ScM of these transitional nuclei to their lowest-lying intrinsic excitations. Furthermore, new representations of both nuclei in the IBM-2, specifically constrained in their choice of the Majorana parameters through these novel data, are presented and discussed. In the particular case of ^{150}Nd a complete determination of all three individual Majorana parameters was accomplished for the first time. Finally, the result of an accordingly updated IBM-2 NME calculations for the $^{150}\text{Nd} \rightarrow {}^{150}\text{Sm}$ $0\nu\beta\beta$ decay is given and again compared with the above-discussed EDF results. Preliminary results have been published in Ref. [22].

Nuclear resonance fluorescence (NRF) experiments [23–26] have been performed on ^{150}Nd and ^{150}Sm using quasimonoenergetic, linearly polarized, γ-ray beams provided by the High Intensity γ-ray Source (HIγS) [27] situated at Duke University in Durham, North Carolina, USA. The two targets were composed of 11.583(1) g of Nd_2O_3 enriched to 93.60(2)% in ^{150}Nd and 2.2791(1) g of Sm_2O_3 enriched to 95.00(2)% in ^{150}Sm, respectively. The fluorescence γ rays were detected by using four high-purity Germanium detectors of the γ^3 setup [28] at HIγS. In the ^{150}Sm experiment these were mounted at a polar angle of $\theta = 90^\circ$ with respect to the beam direction and azimuthal angles of $\phi \in \{0^\circ, 90^\circ, 180^\circ, 270^\circ\}$ with respect to the polarization plane, while in the ^{150}Nd experiment their positions were $(\theta, \phi) \in \{(90^\circ, 180^\circ), (90^\circ, 90^\circ), (135^\circ, 45^\circ), (135^\circ, 135^\circ)\}$. The beam energies were 2994 ± 98 keV for the ^{150}Nd experiment and 3113 ± 131 keV for the ^{150}Sm experiment with the uncertainties representing the full width at half maximum of the beam's nearly Gaussian intensity profile. Each energy was chosen to focus on the respective strongest known ScM state located at this respective energy to study its decay behavior after photoexcitation. While a prior NRF experiment [29] adopted in the nuclear data sheets [30] reported the strongest 1^+_{ScM} state of ^{150}Sm to be at 3082 keV though with tentative parity assignments for all states based on Alaga's rule [31], in our experiment this state was unambiguously assigned negative parity, while the reportedly second strongest ScM state at 3113 keV indeed has positive parity, as reported and required for a ScM state. For ^{150}Nd the previously published $J^\pi = 1^+$ assignment [30,32] of the 2994 keV state could be confirmed. Our parity determinations are based on the strongly differing angular distributions

$$W_{0^+\rightarrow 1^\pm\rightarrow 0^+}(\theta, \phi) = \tfrac{3}{4}[1 + \cos^2(\theta) \pm \sin^2(\theta)\cos(2\phi)] \quad (2)$$

of $0^+ \rightarrow 1^\pm \rightarrow 0^+$ NRF cascades when excited by a linearly polarized γ-ray beam [33,34]. These cause the GS transitions of 1^+ states of even-even nuclei to appear prominently in spectra of detectors placed at $\theta = 90^\circ$ and $\phi \in \{0^\circ, 180^\circ\}$, while rendering them nearly unobservable to detectors at $\theta = 90^\circ$ and $\phi \in \{90^\circ, 270^\circ\}$. As the opposite is true for the GS transitions of 1^- states, parities can immediately be read off the spectra of such placed detectors. Fig. 1 demonstrates this for ^{150}Nd with the 2994 keV state's positive parity being evident through the characteristic azimuthal asymmetry of its GS transition visible in the two spectra.

The strong excitation of the ScM states of interest in both experiments allowed not only to observe their GS transitions, but also their branching transitions into the 2_1^+, 0_2^+, and 2_2^+ states of the respective nucleus, as shown for ^{150}Nd in Fig. 1. Of those only the two 2_1^+ branchings had been observed

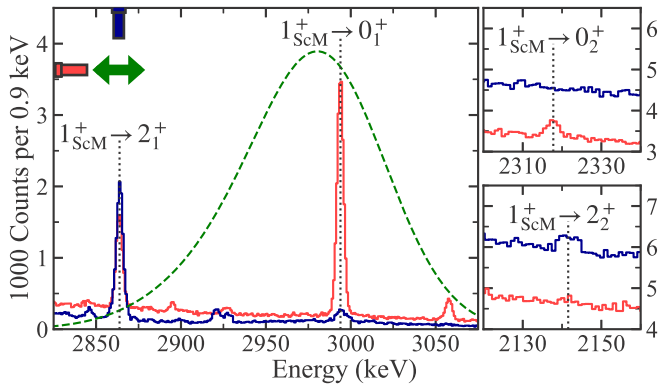

FIG. 1. Three extracts of the ^{150}Nd NRF spectra of the two HPGe detectors placed perpendicular to the beam axis. The color-coded azimuthal detector positions are indicated in the top-left schematic along the γ-ray beam's polarization represented by the green arrow. The here discussed 2994 keV 1^+_{ScM} state's transitions are labeled and the state's positive parity is apparent through the pronounced azimuthal asymmetry of its 0^+ transitions. The green dashed line represents the beam's intensity profile.

before [29,32]. From the $1^+_{ScM} \to 2^+$ transition intensities in the spectra their multipole mixing ratios δ were determined through an angular distribution analysis (in analog to Ref. [35]). While for most transitions this yields two possible δ realizations, in all transitions one δ within its uncertainties is compatible with a nearly pure $M1$ character, as expected for ScM transitions. Hence, in further analysis these smaller-in-magnitude δ values were used. The branching ratios $\Gamma[k]/\Gamma[0^+_1]$ of all observed $1^+_{ScM} \to k$ transitions were determined and are listed in Table I. Here, $\Gamma[k]$ denotes the partial decay width attributed to the $1^+_{ScM} \to k$ transition. The published branching ratios of the previously known $1^+_{ScM} \to 2^+_1$ transitions of ^{150}Nd [32] and ^{150}Sm [29] agree within their larger uncertainties with our results given in Table I. By combining the available energy-integrated cross sections of the $0^+_1 \to 1^+_{ScM} \to 0^+_1$ NRF cascades from Refs. [29,32] with our novel ScM branching ratios, absolute $B(M1)$ transition strengths were calculated for all observed ScM transitions, assuming unobserved transitions to be negligible. The values are listed in Table II. We used these novel data on the decay characteristics of the strongest ScM fragments of ^{150}Nd and ^{150}Sm to improve the representations of these nuclei in the IBM-2, in particular by constraining the IBM-2's Majorana parameters ξ_i. For the calculations we used the program NPBOS [36,37] with the *Talmi-Hamiltonian* [14]

$$H = \epsilon\, n_d + \kappa\, Q^\chi_\pi \cdot Q^\chi_\nu + M_{\pi\nu}(\xi_1, \xi_2, \xi_3), \qquad (3)$$

TABLE I. Branching ratios of investigated 1^+_{ScM} states.

	This work			Refs. [29,32]
Nucleus	$\Gamma[2^+_1]/\Gamma[0^+_1]$	$\Gamma[0^+_2]/\Gamma[0^+_1]$	$\Gamma[2^+_2]/\Gamma[0^+_1]$	$\Gamma[2^+_1]/\Gamma[0^+_1]$
^{150}Nd	0.536(14)	0.0679(48)	0.0530(51)	0.490(44)
^{150}Sm	0.561(41)	0.207(37)	0.171(36)	0.55(8)

TABLE II. Comparison of experimental (Expt.) level energies [30] and $B(M1)$ transition strengths to values calculated with the IBM-2 using the Hamiltonian of Eq. (3) in combination with the parameters given in Table III.

	^{150}Nd		^{150}Sm	
Observable	Expt.	IBM-2	Expt.	IBM-2
$E(2^+_1)$ (keV)	130	130	334	334
$E(4^+_1)$ (keV)	381	381	773	773
$E(0^+_2)$ (keV)	676	676	740	784
$\bar{E}(1^+_{ScM})$ (keV)	3001	3001	3159	3159
$E(6^+_1)$ (keV)	720	739	1279	1317
$E(8^+_1)$ (keV)	1130	1194	1837	1956
$E(10^+_1)$ (keV)	1599	1742	2433	2684
$E(2^+_2)$ (keV)	851	864	1046	1113
$E(4^+_2)$ (keV)	1138	1209	1449	1691
$E(2^+_3)$ (keV)	1062	1039	1194	1446
$B(M1; 1^+_{ScM} \to 0^+_1)$ (μ^2_N)	0.240(26)	0.240	0.072(10)	0.072
$B(M1; 1^+_{ScM} \to 2^+_1)$ (μ^2_N)	0.147(16)	0.163	0.0571(98)	0.0652
$B(M1; 1^+_{ScM} \to 0^+_2)$ (μ^2_N)	0.0351(46)	0.0350	0.0339(83)	0.0713
$B(M1; 1^+_{ScM} \to 2^+_2)$ (μ^2_N)	0.021(11)	0.041	0.040(15)	0.102

where n_d is the total d boson-number operator, Q^χ_π (Q^χ_ν) is the proton (neutron) quadrupole operator,

$$M_{\pi\nu}(\xi_1, \xi_2, \xi_3) = \frac{1}{2}\xi_2(d^\dagger_\nu s^\dagger_\pi - d^\dagger_\pi s^\dagger_\nu)\cdot(\tilde{d}_\nu \tilde{s}_\pi - \tilde{d}_\pi \tilde{s}_\nu) + \sum_{k=1,3} \xi_k\,[d^\dagger_\nu d^\dagger_\pi]^{(k)} \cdot [\tilde{d}_\pi \tilde{d}_\nu]^{(k)} \qquad (4)$$

is the Majorana operator, which mainly affects MSSs like the ScM [20,21], and $\epsilon \geqslant 0$, $\kappa \leqslant 0$, $-\frac{\sqrt{7}}{2} \leqslant \chi \leqslant \frac{\sqrt{7}}{2}$, $\xi_1 \geqslant 0$, $\xi_2 \geqslant 0$, and $\xi_3 \geqslant 0$ are parameters which are adapted to the experimental data. For a systematic determination of these parameters, the following criteria were employed: The calculated energies of the 2^+_1 and 4^+_1 states and of the ScM (1^+_1 in the IBM-2) are required to match within 1 keV to experiment [for the experimentally fragmented ScM a weighted average

$$\bar{E}(1^+_{ScM}) = \frac{\sum E(1^+_{ScM})\; B(M1;\; 1^+_{ScM} \to\; 0^+_1)}{\sum B(M1;\; 1^+_{ScM} \to\; 0^+_1)}$$

was used] and the energy of the 0^+_2 state should be reproduced as close as possible. With these criteria ϵ, κ, χ, and one degree of freedom (DOF) in the Majorana parameters ξ_i, considered as a total *Majorana strength* $\xi_1{+}\xi_2{+}\xi_3$, are virtually fixed for ^{150}Nd and ^{150}Sm, leaving only two DOF in distributing this total Majorana strength along its three subterms. Rewriting these as ratios $x_2 = \frac{\xi_2}{\xi_1+\xi_2+\xi_3}$ and $x_1 = \frac{\xi_1}{\xi_1+\xi_3}$ with $0 \leqslant x_i \leqslant 1$, their effect on the ScM's decay behavior was systematically studied by performing IBM-2 calculations (for ^{150}Nd and ^{150}Sm each) spanning a grid in this x_1-x_2 plane. In all these calculations the remaining virtually fixed parameters (fixed with respect to a specific choice of the x_i) were set according to the aforementioned criteria, hence precluding any effects purely from changes of energies of the low-lying states and the ScM. The result of this investigation for ^{150}Nd is visualized in Fig. 2. The $1^+_{ScM} \to 0^+_2$ transition's branching ratio, in the

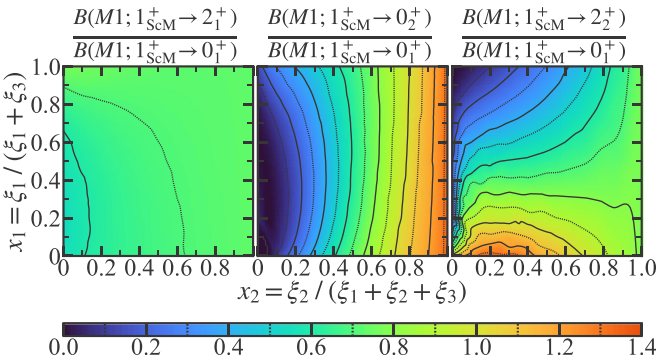

FIG. 2. Dependence of the ScM's $M1$ decay behavior in IBM-2 calculations of ^{150}Nd on the relative strengths x_i of the Majorana parameters ξ_i. Each contour plot interpolates the dependence of one relative $B(M1)$ strength stated at its top and extracted from IBM-2 calculations on a grid with the remaining DOF in each calculation chosen to reproduce the level structure of ^{150}Nd.

form of a $B(M1)$ ratio varying from zero up to 1.4, is found to be sensitive to the x_2 DOF, but barely to x_1. The $1^+_{ScM} \to 2^+_2$ branching ratio with about the same value range is sensitive to a combination of both x_2 and x_1. The $1^+_{ScM} \to 2^+_1$ branching is barely sensitive to either. For ^{150}Sm a qualitatively similar result (though with different slopes and value ranges of the $B(M1)$ ratios) is obtained, yielding identical sensitivities. Hence, a determination of all three Majorana parameters can be achieved from combined data on the ScM's energy and its 0^+_2 and 2^+_2 branching ratios.

Using this finding along with the stated criteria, new IBM-2 parameter sets for ^{150}Nd and ^{150}Sm were derived. The parameter sets can be found in Table III and a comparison to experiment is given in Table II and Fig. 3. In both calculations the experimental energies of the respective 2^+_1, 4^+_1, and 1^+_{ScM} states were reproduced with deviations less than 1 keV as intended. For ^{150}Nd this was also achieved for the 0^+_2 state, while for ^{150}Sm the calculated 0^+_2 energy is about 6% too high due to the parameter χ reaching its lower limit. Comparing the calculations to further experimental data on

TABLE III. IBM-2 Hamiltonian parameters derived in this work.

Nucleus	ϵ (keV)	κ (keV)	χ	ξ_1 (keV)	ξ_2 (keV)	ξ_3 (keV)
^{150}Nd	481.5	−77.06	−0.9903	1221	139.8	293.0
^{150}Sm	747.6	−75.15	−1.323	885.2	196.7	885.2

level energies and $B(E2)$ transition strengths available in the nuclear data sheets [30] yields a remarkable agreement for ^{150}Nd considering the simplicity of the Hamiltonian used: All relative deviations in level energies shown in Table II are below 9% and the $B(E2)$ transition strengths are mostly well reproduced although not fit apart from scale. While for ^{150}Sm the overall agreement is slightly worse, the data are still well reproduced and most level energies deviate only by a few percent. Considering the decay behavior of the ScM, the IBM-2 reproduces our new experimental data on ^{150}Nd remarkably well: While its $B(M1; 1^+_{ScM} \to 0^+_1)$ is trivially matched to set the absolute scaling of the transition strengths in terms of the effective boson g factors, its $B(M1; 1^+_{ScM} \to 0^+_2)$ is reproduced exactly through tuning of the x_2 DOF, its $B(M1; 1^+_{ScM} \to 2^+_1)$ is matched within its uncertainty and $B(M1; 1^+_{ScM} \to 2^+_2)$ is brought comparably close to the experimental value by tuning x_1. Hence, for ^{150}Nd our new data on the decay characteristics of the ScM for the first time allowed us to determine all three IBM-2 Majorana parameters individually (instead of only constraining two DOF as previously done in Ref. [10] for ^{154}Gd) using a novel systematic investigation of their effect in the model. For the more vibrational nucleus ^{150}Sm, however, the situation is more complex. Optimizing the x_2 DOF of the Majorana parameters with respect to the $B(M1; 1^+_{ScM} \to 0^+_2)$ of ^{150}Sm causes ξ_2 to reach its lower limit of zero, eliminating the respective Majorana operator term altogether, even before the experimental $B(M1; 1^+_{ScM} \to 0^+_2)$ is reached. More seriously, setting $\xi_2 = 0$ causes MSSs to appear at implausibly low excitation energies in the calculation, e.g., a 2^+ MSS at 1183 keV and a 4^+ MSS at 1546 keV. Such energetically low MSSs have not been observed and would be untypical for a

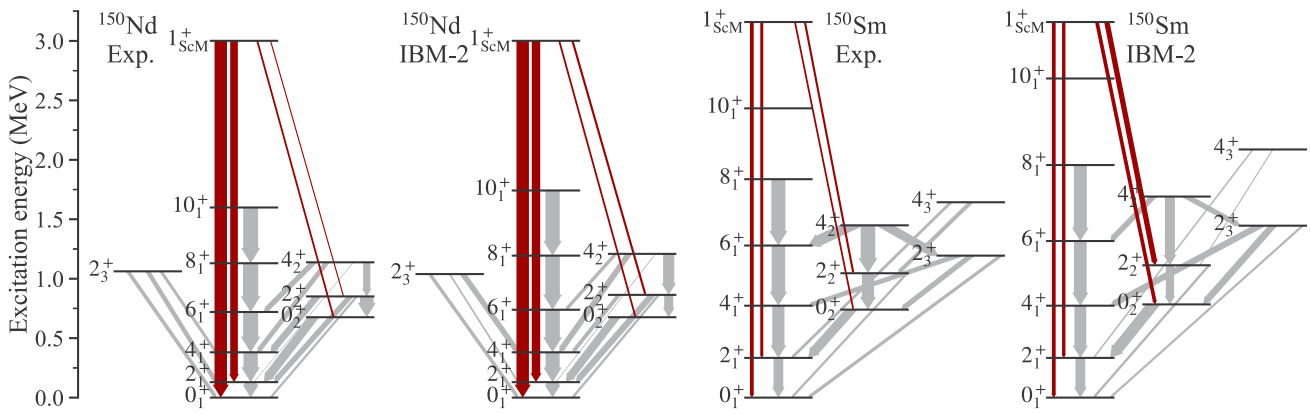

FIG. 3. Comparison of our IBM-2 calculations [using the Hamiltonian of Eq. (3) with its parameters given in Table III] with experimental values for ^{150}Nd and ^{150}Sm. The dark-red arrows represent the newly obtained $M1$ transition strengths [linewidths $\propto B(M1)$], the light gray arrows $E2$ transition strengths [linewidths $\propto \sqrt[3]{B(E2)}$]. The $B(E2)$ values and excitation energies were taken from Ref. [30].

collective nucleus [18]. Hence for the presented calculation on ^{150}Sm the x_2 DOF was balanced to $x_2 = 0.1$ to push the MSSs to excitation energies of at least 2 MeV in accordance with near spherical isotopes in this mass region [18], while still reproducing the ScM branching ratios as well as possible. Also no attempt to fit x_1 was made. Instead, ξ_1 and ξ_3 were set equal ($x_1 = \frac{1}{2}$), analogous to previous works in the literature [10]. In conclusion, for ^{150}Sm two of three DOFs in the Majorana parameters were reasonably constrained.

Having acquired these newly constrained parameter sets to represent ^{150}Nd and ^{150}Sm in the IBM-2, a new calculation of the $^{150}\text{Nd} \rightarrow {}^{150}\text{Sm}$ $0\nu\beta\beta$ NMEs was performed by using the existing formalism [13,15]. The results are $M^{(0\nu\beta\beta)}_{\text{IBM-2}}[0^+_1] = 3.35$ for the $0\nu\beta\beta$ decay to the GS of ^{150}Sm and $M^{(0\nu\beta\beta)}_{\text{IBM-2}}[0^+_2] = 1.30$ for the decay to its 0^+_2 state. Hence, compared with the previous IBM-2 calculation [15] the NME for the GS decay changed by about 11 %, while the NME for the 0^+_2 decay grew by more than a factor of two. Although this lessens the discrepancy between IBM-2 and EDF calculations, the deviation to the EDF results of $M^{(0\nu\beta\beta)}_{\text{EDF}}[0^+_1] = 1.71$ and $M^{(0\nu\beta\beta)}_{\text{EDF}}[0^+_2] = 2.81$ [10] is still significant. In particular, the two approaches disagree on the transition of largest NME, as the IBM-2 calculation predicts the NME for the $0\nu\beta\beta$ decay to the GS of ^{150}Sm to be larger than the NME for a decay into the 0^+_2 state, while the EDF predicts the opposite. This discrepancy is likely founded in differing descriptions of the three 0^+ states involved between the models: When the wave function overlap between mother and daughter states is large, the $0\nu\beta\beta$ NME can be expected to be large [11]. In the $N \approx 90$ spherical-deformed shape-phase transition region this can be discussed by means of spherical and deformed configurations and their mixture into the wave functions of the 0^+ states. The amount of mixing depends on the height of the potential barrier between both configurations and the mixing matrix element. This delicate balance appears to come out differently in the models at hand.

The situation can be addressed qualitatively. In the IBM, a strong mixing between the lowest 0^+ states is known to occur at the shape-phase transition. This is seen in multiple avoided crossings of 0^+ states across the shape-phase transition for finite boson numbers [38,39]. ^{150}Nd is closest to the critical point of the transition; hence, spherical and deformed configurations can be expected to mix into both the GS and 0^+_2 state. In comparison, the more spherical ^{150}Sm should have little deformed configuration in its GS and excited-state wave functions—rather, its excited 0^+_2 state should have a dominant two-phonon nature, which, in turn, is lacking in the ^{150}Nd GS. Hence, in this picture a mixed GS of ^{150}Nd has less overlap with the 0^+_2 state of ^{150}Sm than with its GS.

The EDF result of Ref. [10], on the other hand, predicts a stronger $0\nu\beta\beta$ decay into the 0^+_2 state of ^{150}Sm, pointing to a larger overlap of its wave function with the GS of ^{150}Nd. This points rather to a shape-coexistence picture, where a spherical and a deformed configuration exchange roles, hence, a more deformed GS of ^{150}Nd could have a larger overlap with its partner in ^{150}Sm, i.e., its 0^+_2 state, consequently leading to this $0\nu\beta\beta$ decay path being preferred.

Overall, one can expect the challenging description of the delicate interplay, exchange of and mixing between spherical and deformed configurations in this shape-phase transitional region to be the cause for the quite different predictions of the models.

In summary, two NRF experiments were performed at HIγS to study the decay behavior of the strongest 1^+ ScM fragments in the $0\nu\beta\beta$-partner nuclides ^{150}Nd and ^{150}Sm. For both nuclei, and for the first time in transitional nuclei, transitions of the ScM to the 0^+_2 and 2^+_2 states were observed and the respective branching ratios determined. By performing a systematic investigation in the IBM-2 a sensitivity of these two branching ratios on the model's Majorana DOF was established, which in combination with the experimental excitation energy of the ScM in principle allows us to determine all three Majorana parameters of a nucleus in the IBM-2 individually. Using this finding and the novel data, new IBM-2 parameter sets for both nuclei were derived, which in particular incorporate constraints on the Majorana parameters. For ^{150}Nd a definite determination of all three of its Majorana parameters was achieved with an overall remarkably well matching IBM-2 calculation. While for ^{150}Sm the model has slight difficulties to fully reproduce the experimental data, nevertheless two of three DOF in its Majorana parameters were reasonably constrained. Finally, these two newly constrained IBM-2 representations were employed in a recalculation of the $^{150}\text{Nd} \rightarrow {}^{150}\text{Sm}$ $0\nu\beta\beta$-decay NMEs, which in particular now yields more than double the previous IBM-2 value for the NME of the $0\nu\beta\beta$ decay into the 0^+_2 state of ^{150}Sm. Although this lessened the discrepancy between IBM-2 and EDF calculations of the NMEs, they still differ significantly. Presumably, this is due to differing descriptions of the spherical-deformed shape-phase transition in the $N \approx 90$ region and its effects on the structure of the 0^+ states involved.

We thank the HIγS accelerator crew for providing perfect conditions for our experiments. The ^{150}Nd target was supplied by the Isotope Program within the Office of Nuclear Physics in the U.S. Department of Energy's Office of Science. This work has been funded by the German state of Hesse under the grant "Nuclear Photonics" within the LOEWE program, by the Deutsche Forschungsgemeinschaft (DFG, German Research Foundation) - Project-ID 279384907 - SFB 1245, by the German Federal Ministry of Education and Research (BMBF) under Grant No. 05P18RDEN9, by the U.S. Department of Energy, Office of Nuclear Physics, under Grant No. DE-FG02-97ER41033, and by the Academy of Finland, Grants No. 314733 and No. 320062. J.K., T.B., U.F.-G., and O.P. acknowledge support by the Helmholtz Graduate School for Hadron and Ion Research of the Helmholtz Association.

[1] J. D. Vergados, H. Ejiri, and F. Šimkovic, Rep. Prog. Phys. **75**, 106301 (2012).

[2] F. T. Avignone, S. R. Elliott, and J. Engel, Rev. Mod. Phys. **80**, 481 (2008).

[3] M. J. Dolinski, A. W. P. Poon, and W. Rodejohann, Annu. Rev. Nucl. Part. Sci. **69**, 219 (2019).

[4] S. R. Elliott and P. Vogel, Annu. Rev. Nucl. Part. Sci. **52**, 115 (2002).

[5] J. Engel and J. Menéndez, Rep. Prog. Phys. **80**, 046301 (2017).

[6] K. Zuber, Consensus report of a workshop on "matrix elements for neutrinoless double beta decay," arXiv:nucl-ex/0511009.

[7] R. F. Casten, Nat. Phys. **2**, 811 (2006).

[8] R. Krücken, B. Albanna, C. Bialik, R. F. Casten, J. R. Cooper, A. Dewald, N. V. Zamfir, C. J. Barton, C. W. Beausang, M. A. Caprio, A. A. Hecht, T. Klug, J. R. Novak, N. Pietralla, and P. von Brentano, Phys. Rev. Lett. **88**, 232501 (2002).

[9] R. F. Casten and N. V. Zamfir, Phys. Rev. Lett. **87**, 052503 (2001).

[10] J. Beller, N. Pietralla, J. Barea, M. Elvers, J. Endres, C. Fransen, J. Kotila, O. Möller, A. Richter, T. R. Rodríguez, C. Romig, D. Savran, M. Scheck, L. Schnorrenberger, K. Sonnabend, V. Werner, A. Zilges, and M. Zweidinger, Phys. Rev. Lett. **111**, 172501 (2013).

[11] T. R. Rodríguez and G. Martínez-Pinedo, Phys. Rev. Lett. **105**, 252503 (2010).

[12] O. Scholten, F. Iachello, and A. Arima, Ann. Phys. (NY) **115**, 325 (1978).

[13] J. Barea and F. Iachello, Phys. Rev. C **79**, 044301 (2009).

[14] F. Iachello and A. Arima, *The Interacting Boson Model*, Cambridge Monographs on Mathematical Physics (Cambridge University Press, Cambridge, UK, 1987).

[15] F. F. Deppisch, L. Graf, F. Iachello, and J. Kotila, Phys. Rev. D **102**, 095016 (2020).

[16] F. Iachello, Phys. Rev. Lett. **53**, 1427 (1984).

[17] P. V. Isacker, K. Heyde, J. Jolie, and A. Sevrin, Ann. Phys. (NY) **171**, 253 (1986).

[18] N. Pietralla, P. von Brentano, and A. F. Lisetskiy, Prog. Part. Nucl. Phys. **60**, 225 (2008).

[19] K. Heyde, P. von Neumann-Cosel, and A. Richter, Rev. Mod. Phys. **82**, 2365 (2010).

[20] F. Iachello and I. Talmi, Rev. Mod. Phys. **59**, 339 (1987).

[21] O. Scholten, K. Heyde, P. van Isacker, J. Jolie, J. Moreau, M. Waroquier, and J. Sau, Nucl. Phys. A **438**, 41 (1985).

[22] U. Friman-Gayer, Ph.D. thesis, Technische Universität Darmstadt, Germany, 2020.

[23] U. Kneissl, H. H. Pitz, and A. Zilges, Prog. Part. Nucl. Phys. **37**, 349 (1996).

[24] U. Kneissl, N. Pietralla, and A. Zilges, J. Phys. G **32**, R217 (2006).

[25] F. R. Metzger, Prog. Nucl. Phys. **7**, 54 (1959).

[26] N. Pietralla, J. Isaak, and V. Werner, Eur. Phys. J. A **55**, 237 (2019).

[27] H. R. Weller, M. W. Ahmed, H. Gao, W. Tornow, Y. K. Wu, M. Gai, and R. Miskimen, Prog. Part. Nucl. Phys. **62**, 257 (2009).

[28] B. Löher, V. Derya, T. Aumann, J. Beller, N. Cooper, M. Duchêne, J. Endres, E. Fiori, J. Isaak, J. Kelley, M. Knörzer, N. Pietralla, C. Romig, D. Savran, M. Scheck, H. Scheit, J. Silva, A. Tonchev, W. Tornow, H. Weller *et al.*, Nucl. Instrum. Methods Phys. Res., Sect. A **723**, 136 (2013).

[29] W. Ziegler, N. Huxel, P. von Neumann-Cosel, C. Rangacharyulu, A. Richter, C. Spieler, C. D. Coster, and K. Heyde, Nucl. Phys. A **564**, 366 (1993).

[30] S. K. Basu and A. A. Sonzogni, Nucl. Data Sheets **114**, 435 (2013).

[31] G. Alaga, K. Alder, A. Bohr, and B. R. Mottelson, Dan. Mat. Fys. Medd. **29**, 1 (1955).

[32] H. H. Pitz, R. D. Heil, U. Kneissl, S. Lindenstruth, U. Seemann, R. Stock, C. Wesselborg, A. Zilges, P. von Brentano, S. D. Hoblit, and A. M. Nathan, Nucl. Phys. A **509**, 587 (1990).

[33] N. Pietralla, Z. Berant, V. N. Litvinenko, S. Hartman, F. F. Mikhailov, I. V. Pinayev, G. Swift, M. W. Ahmed, J. H. Kelley, S. O. Nelson, R. Prior, K. Sabourov, A. P. Tonchev, and H. R. Weller, Phys. Rev. Lett. **88**, 012502 (2001).

[34] L. W. Fagg and S. S. Hanna, Rev. Mod. Phys. **31**, 711 (1959).

[35] T. Beck, J. Beller, N. Pietralla, M. Bhike, J. Birkhan, V. Derya, U. Gayer, A. Hennig, J. Isaak, B. Löher, V. Y. Ponomarev, A. Richter, C. Romig, D. Savran, M. Scheck, W. Tornow, V. Werner, A. Zilges, and M. Zweidinger, Phys. Rev. Lett. **118**, 212502 (2017).

[36] T. Otsuka, O. Scholten, and N. Yoshida, Computer program NPBOS (1976–1985).

[37] T. Otsuka and N. Yoshida, *User's manual of the program NPBOS*, Tech. Rep. JAERI-M/85-094 (Japan Atomic Energy Research Institute, 1985).

[38] P. Cejnar, S. Heinze, and J. Jolie, Phys. Rev. C **68**, 034326 (2003).

[39] D. A. Meyer, V. Wood, R. F. Casten, C. R. Fitzpatrick, G. Graw, D. Bucurescu, J. Jolie, P. von Brentano, R. Hertenberger, H.-F. Wirth, N. Braun, T. Faestermann, S. Heinze, J. L. Jerke, R. Krücken, M. Mahgoub, O. Möller, D. Mücher, and C. Scholl, Phys. Rev. C **74**, 044309 (2006).